A Computational Model for Short-Wavelength Stall Inception and Development in Multistage Compressors

Y. Gong

C. S. Tan

K. A. Gordon

Gas Turbine Laboratory,
Massachusetts Institute of Technology,
Cambridge, MA 02139

E. M. Greitzer[1]
United Technologies Research Center,
East Hartford, CT 06108

This paper presents a computational model for simulating axial compressor stall inception and development via disturbances with length scales on the order of several (typically about three) blade pitches. The model was designed for multistage compressors in which stall is initiated by these "short-wavelength" disturbances, also referred to as spikes. The inception process described is fundamentally nonlinear, in contrast to the essentially linear behavior seen in so-called "modal stall inception." The model was able to capture the following experimentally observed phenomena: (1) development of rotating stall via short-wavelength disturbances, (2) formation and evolution of localized short-wavelength stall cells in the first-stage of a mismatched compressor, (3) the switch from long to short-wavelength stall inception resulting from the re-staggering of the inlet guide vane, (4) the occurrence of rotating stall inception on the negatively sloped portion of the compressor characteristic. Parametric investigations indicated that: (1) short-wavelength disturbances were supported by the rotor blade row, (2) the disturbance strength was attenuated within the stators, and (3) the reduction of inter-blade row gaps can suppress the growth of short-wavelength disturbances. It is argued that each local component group (rotor plus neighboring stators) has its own instability point (i.e., conditions at which disturbances are sustained) for short-wavelength disturbances, with the instability point for the compressor set by the most unstable component group.

Introduction

Experiments performed on compressor rigs (Day, 1993; Longley et al., 1996; Silkowski, 1995; Tryfonidis et al., 1995; Weigl et al., 1996; Camp and Day, 1998) and engines (Day et al., 1999) have demonstrated that there are two routes to rotating stall in axial compressors. The first is characterized by the growth of small-amplitude, essentially two-dimensional long wavelength disturbances (on the order of the circumference), which extend axially through the compressor. These disturbances, referred to as modal stall waves, can be detected from 10 to more than 100 rotor revolutions prior to stall, and they rotate at 0.2 to 0.5 times the rotor speed (McDougall, 1988; Haynes et al., 1994; Tryfonidis et al., 1995). Two-dimensional linearized stability analyses (Moore, 1984; Moore and Greitzer, 1986; Weigl et al., 1998) give a useful description of the modal wave shape, phase speed, and growth rate for many compressors.

The second route to rotating stall is characterized by the development of three-dimensional "spike" disturbances (Day, 1993; Silkowski, 1995). These are localized to the tip region of a specific rotor in a multistage compressor and have a length scale on the order of the blade pitch. Spikes initially rotate at 0.7 to 0.8 times the rotor speed, but slow to 0.2 to 0.5 times the rotor speed as they develop into a full stall cell. The time between first detecting a spike and the final stall cell is less than five rotor revolutions, much shorter than for modal-type stall development.

Short wavelength stall inception behavior cannot be captured by current linearized stability analyses. Isolated rotor calculations performed by Hoying et al. (1999) have shown a causal link between the rotor tip leakage flow and the *formation* of the

incipient spike disturbances found in experiments, but the calculations do not provide a framework by which to examine the *development* of these localized flow events into rotating stall. Furthermore, there is currently no methodology for assessing the controlling design parameters and conditions that set the stalling behavior of a multistage compressor with short wavelength disturbances. It is the lack of such capabilities that motivated us to undertake the work presented in this paper.

The technical goal was to develop the simplest computational flow model with the capability of simulating both types of stall inception and development in a multistage axial compressor, and use the model to assess the effect of design parameters on the compressor stability to short-wavelength disturbances. To put it in another way, what we have done is to first postulate a scenario for the development of short-wavelength stall inception, work out rigorously the consequences of this scenario, subject these consequences to scrutiny using available experiments and analysis, and, based on the results, use the model to infer parametric trends for the phenomena of interest.

The paper is organized as follows: We first describe the formulation of the computational model and the procedure for using the model to simulate stall inception. Model adequacy is assessed by comparison with two- and three-dimensional linearized stability analyses and experimental data of short-wavelength stalling behavior in matched and mismatched compressors. The model is then applied to explore the design parameters and conditions that control the stalling behavior of a multistage axial compressor. The implications of these results on the two different routes to rotating stall are discussed by developing the "local component group" concept, and relating this concept to the recent short-wavelength stall arguments set forth by Hoying et al. (1999) and Camp and Day (1998).

Computational Model

To simulate short-wavelength disturbances, a model must be capable of describing the three-dimensional and nonlinear aspects

Copyright © 1999 by ASME

axisymmetric Euler with body force

upstream duct   compressor   downstream duct   plenum   throttle

computational domain

Fig. 1 Illustration of the blade row model in the compression system

$$\frac{\partial}{\partial t}\begin{bmatrix} 0 \\ rV_x \\ rV_\theta \\ rV_r \end{bmatrix} + \frac{\partial}{\partial x}\begin{bmatrix} rV_x \\ rV_x^2 + rP/\rho \\ rV_xV_\theta \\ rV_xV_r \end{bmatrix} + \frac{\partial}{\partial\theta}\begin{bmatrix} V_\theta \\ V_\theta V_x \\ V_\theta^2 + P/\rho \\ V_\theta V_r \end{bmatrix}$$

$$+ \frac{\partial}{\partial r}\begin{bmatrix} rV_r \\ rV_xV_r \\ rV_\theta V_r \\ rV_r^2 + rP/\rho \end{bmatrix} = \begin{bmatrix} 0 \\ 0 \\ -V_\theta V_r \\ V_\theta^2 + P/\rho \end{bmatrix} \tag{1}$$

Blade Rows. The pressure rise and the turning produced by each blade row were modeled by a body force field, distributed continuously around the circumference (Fig. 1). The blade region is assumed to consist of an infinite number of blades, which restrict circumferential flow variations from redistributing. Tangential flow gradients can exist, but they do not affect the local flow dynamics in the blade row reference frame. The relative flow was therefore described by "locally axisymmetric" Euler equations with source terms depicting the body forces. In the absolute frame, these equations are given by

$$\left(\frac{\partial}{\partial t} + \Omega\frac{\partial}{\partial\theta}\right)\begin{bmatrix} 0 \\ rV_x \\ rV_\theta \\ rV_r \end{bmatrix} + \frac{\partial}{\partial x}\begin{bmatrix} rV_x \\ rV_x^2 + rP/\rho \\ rV_xV_\theta \\ rV_xV_r \end{bmatrix}$$

$$+ \frac{\partial}{\partial r}\begin{bmatrix} rV_r \\ rV_xV_r \\ rV_\theta V_r \\ rV_r^2 + rP/\rho \end{bmatrix} = \begin{bmatrix} 0 \\ rF_x \\ -V_\theta V_r + rF_\theta \\ V_\theta^2 + P/\rho + rF_r \end{bmatrix} \tag{2}$$

where

$$(F_x, F_\theta, F_r) = \mathbf{F}(\mathbf{V}(x, \theta, r), x, r). \tag{3}$$

The additional operator $\Omega\partial/\partial\theta$ in Eq. (2) arises from the transformation of the time derivative from the rotational frame to the absolute frame. The assumption of an infinite number of blades is well based for perturbations with wavelengths much longer than the blade pitch (such as modal waves). For short-wavelength disturbances, tangential redistribution within individual blade passages would be expected. The applicability of the model to simulate these disturbances will be made apparent during the model assessment.

With short-wavelength spikes there is a potential for substantial axial and radial flow redistribution within the blade row. The body force field accounts for this at every point in the blade region by responding to the local flow conditions. This contrasts with previous body force representations (Escuret and Garnier, 1994; Longley, 1997) in which the force responded only to the flow at the blade row inlet. Details of how local body force relations were generated from prescribed axisymmetric pressure rise and turning characteristics are given in the appendix.

Plenum and Throttle. Standard plenum and throttle dynamics were used to determine the pressure at the exit of the downstream duct (Greitzer, 1976). Since the plenum has little effect on

of the flow in a multistage environment. Direct use of a three-dimensional unsteady Navier–Stokes solver to compute the flow within all blade passages of a compressor is not computationally feasible, nor is it suited to our requirements. The approach taken here is to use body force distributions to represent the effects of the discrete blades on the flow field.

The body force approach is not new (Marble, 1964; Billet et al., 1988) and has been recently used by Escuret and Garnier (1994) and Longley (1997) to simulate the onset of rotating stall from long-wavelength disturbances. The work presented here constitutes the first effort, as far as the authors know, to exploit the potential for simulating three-dimensional nonlinear instability for short-wavelength disturbances in multistage compressors.

The modeled compression system consisted of an inlet duct, blade rows, inter-blade row gaps, an exit duct, and a plenum followed by a throttle (Fig. 1). The computational domain extended to the end of the downstream duct where the exit pressure was determined by the plenum and throttle dynamics. The flow was assumed to be incompressible, consistent with the low-speed compressor experiments against which the model was compared. Key elements for modeling each component are detailed in the following subsections.

Upstream Duct, Downstream Duct and Gaps. Flow in the blade-free regions was described by the unsteady three-dimensional Euler equations:

Nomenclature

F = body force per unit mass
K_t = throttle coefficient
P = static pressure
U = midspan blade speed
V = velocity
c = pseudo-speed of sound
x, θ, r = cylindrical coordinates

α = blade metal angle
β = flow angle = tan $(\beta) = V_\theta/V_x$
δ = loss of stall margin, defined by Eq. (5)
ρ = density
ϕ = flow coefficient = V_x/U
Ψ_{ts} = total-to-static pressure rise = $(P_{exit} - P_{t,inlet})/\rho U^2$

Ψ_{tt} = total-to-total pressure rise = $(P_{t,exit} - P_{t,inlet})/\rho U^2$
Ω = rotating frequency of the blade rows

Subscripts

t = stagnation property
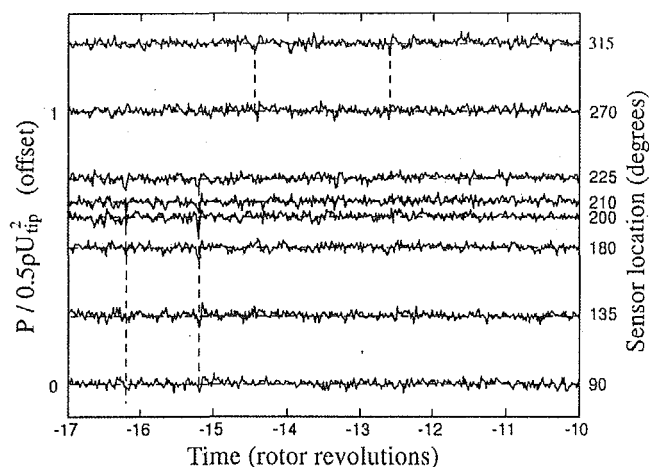x, θ, r = axial, circumferential, radial component

Fig. 2 Experimental evidence of tip-spikes prior to the development of stall at time = 0. The pressure traces, from sensors at different circumferential positions, are shifted relative to first trace so that disturbances traveling at 71 percent of rotor speed line up vertically. Guide lines identify propagating spikes (Park, 1994).

Fig. 3 Axial body force impulse used to generate spike-shaped disturbances

the development of short-wavelength disturbances, its volume was set to zero for the calculations reported, so the exit pressure was determined by the throttle relation

$$P_{\text{exit}} - P_{\text{ambient}} = K_t \phi^2 \qquad (4)$$

where P_{exit} is the pressure at the exit of the downstream duct.

Numerical Method. To allow for a standard time-marching method, a pseudo-compressibility term, $(\partial/\partial t + \Omega\partial/\partial\theta)rP/c^2\rho$, was added to the mass conservation equation. It was found that the phase speeds and growth rates of disturbances were not sensitive to c when c is sufficiently large ($c > 10\phi$). Spatial discretization of the governing equations was based on the finite volume method of Jameson et al. (1981). Since these were low-speed calculations, only fourth-order numerical smoothing was used. The temporal discretization used the four-stage Runge–Kutta scheme with a uniform time step to ensure a time-accurate solution.

Implementation of the Model for Compressor Instability Simulations

This section addresses three issues concerning the use of the model to investigate compressor instability behavior: (1) appropriate initial flow disturbances used for initiating rotating stall, (2) the method for determining the stall point, and (3) the procedure for differentiating between the two stall inception routes.

Two types of initial flow disturbance were used in the calculations. Long-wavelength perturbations of small amplitude (less than 1 percent of the mean flow coefficient) were used to find the modal (linear) stability point. All other calculations used large-amplitude spikes of small circumferential extent that were localized at the tip region of a rotor blade row. These spikes were based on the experimental observations by Park (1994) that such disturbances can appear in a rotor prior to the development of rotating stall (Fig. 2).

The spike disturbances were generated by prescribing an impulse to the rotor axial body force lasting for 0.1 rotor revolutions and traveling at the rotor speed. A disturbance was initiated at a random position about the circumference once every few rotor revolutions. The shape of the impulse (Fig. 3) was approximately 10 deg wide, corresponding to about one blade passage in a 54-blade rotor. The magnitude of the force was equivalent to that effecting zero pressure rise in the outer 30 percent span of a blade passage, which was observed to precede stall in the simulations calculated by Hoying et al. (1999) and Vo (1999).
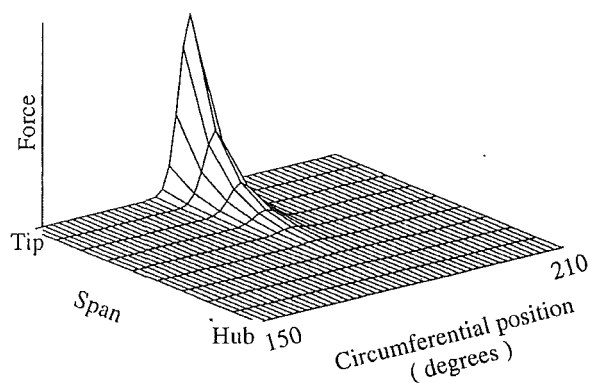
To determine the compressor stall point, the disturbances were first imposed on a steady flow at a fixed throttle coefficient known to produce a stable flow field. This procedure was repeated for lower throttle conditions until the disturbances no longer decayed, but rather grew into a full stall cell. A single simulation with a continuously closing throttle was avoided because any numerically acceptable closing rate would still be much faster than that used in experiments.

Once the stall point was determined, velocity traces were used to determine the route by which the stall cell formed. Long-wavelength inception was characterized by decay of the spike disturbance followed by growth of a long wavelength stall cell. Figure 4 shows an example of flow coefficient traces leading to stall via this route. It is noted that this is not identical to modal stall behavior due to the large amplitude of the initial disturbance. For short wavelength stall inception (Fig. 5) the spike disturbance shape remained coherent and led directly to stall without decay.

Model Assessment

The adequacy of the model and the above-described methodology were assessed by demonstrating that the model reproduced: (1) modal stall behavior as predicted by linearized stability calculations, and (2) experimentally observed short-wavelength instability phenomena. The short-wavelength stall assessments address the question of whether a model based on the assumption of an infinite number of blades can be employed to describe flow events with a length scale of only two to three blade passages.

Three multistage experiments involving short-wavelength disturbances were used for the latter assessment. The first showed a
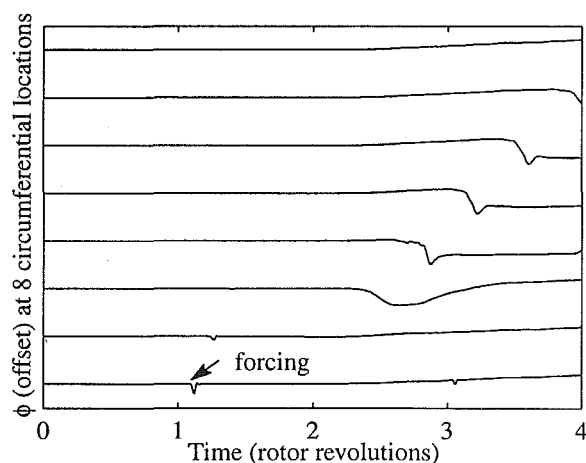

Fig. 4 Computed flow coefficient traces for a compressor stalling via long-wavelength route
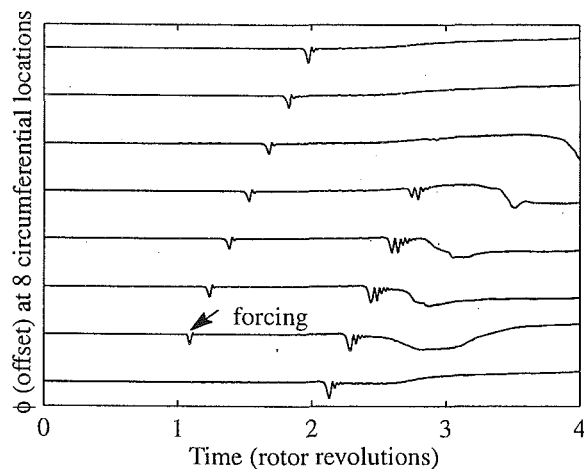
Fig. 5 Computed flow coefficient traces at the tip of the first rotor inlet for a compressor stalling via short-wavelength route

spike disturbance developing into full-scale rotating stall in a matched compressor. The second showed the localization of three-dimensional stall cells in the first stage of a mismatched compressor. The third showed a change from long-wavelength to short-wavelength stall inception routes as the incidence on the first rotor was increased; thereafter, short-wavelength stall inception occurred at a constant rotor tip incidence.

All calculations used 9 radial and 256 circumferential cells. Short-wavelength events occupying two to three blade pitches in the experiments were adequately resolved over 10 to 14 cells in the tangential direction.

Comparisons With Linear Theories. The computational model was first compared separately against two-dimensional and three-dimensional linearized theories for representative compressor geometries. The figures of merit were the growth rate and phase speed of an imposed sinusoidal perturbation with a wavelength equal to the circumference. The two-dimensional case used the parameters similar to a four-stage core compressor. The three-dimensional validation used the geometry of a single-stage fan with a hub-to-tip ratio of 0.43. Computed growth rates and phase speeds are compared in Table 1 with results of two-dimensional (Moore and Greitzer, 1986) and three-dimensional linearized models.

The excellent quantitative agreement between the computational model and the linearized analyses demonstrate that the present method can accurately capture modal instability inception and development. The more important aspect is the additional ability to reproduce short wavelength events, which we proceed to demonstrate next.

Simulation of Short-Wavelength Stall Inception. Measurements of short-wavelength disturbances growing into fully developed rotating stall in a low-speed compressor (Silkowski, 1995) were used as an experimental assessment of the computational model. The compressor (run at the General Electric Aerodynamics Research Laboratory) had a hub-to-tip ratio of 0.85, and consisted

Table 1 Comparison between modal growth rates and phase speeds for the present computational model and linearized analyses

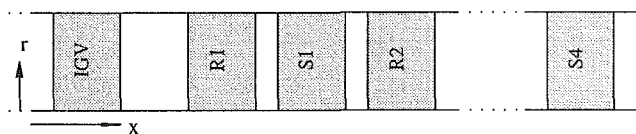|	growth rate	phase speed / rotor speed
Computational model	-0.26	0.27
2D linear model	-0.26	0.27
Computational model	-0.11	0.10
3D linear model	-0.10	0.10

Fig. 6 A scale schematic of the GE compressor represented by nine blade rows and eight gaps

of an inlet guide vane (IGV) followed by four identical stages. A schematic that shows the scale of the blades and interblade axial gaps is given in Fig. 6. Details of the compressor geometry can be found from Wisler (1981).

The pressure rise characteristics used for every rotor and stage in the model are shown in Fig. 7. The rotor characteristic were higher at the tip than the hub to satisfy radial equilibrium at the rotor exit with a nearly uniform axial velocity profile, which was observed in the experiment. The unstalled portions (to the right of the peaks) were taken directly from the experiment. The criteria for selecting the characteristic shapes to the left of the peak, as well as information on their effect on short wavelength stall phenomena, are provided by Gong (1998). The point to be emphasized is that the qualitative stalling behavior is not strongly dependent on the precise curve shapes, other than the requirement that a trough exist in the rotor characteristic at a positive flow coefficient.

This compressor stalled via short-wavelength disturbances, as shown by the axial velocity traces around the circumference (Fig. 8). The computational model qualitatively reproduced this behavior, as shown by the flow coefficient traces in Fig. 5, which are plotted to the same time scale. The same feature of a spike-shaped disturbance growing in amplitude prior to the formation of a fully developed stall cell is shown. Table 2 quantitatively summarizes the key figures of merit used for the assessment. Specifically, the rotating speed of the spike and the time taken for the spike to transition to the final stall cell were in good agreement.
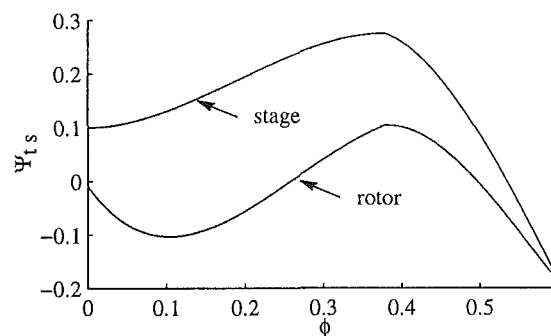

Fig. 7 The modeled axisymmetric pressure rise characteristic for each stage of the GE matched compressor
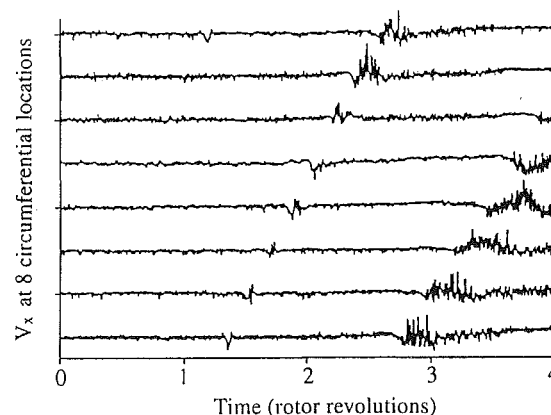

Fig. 8 Measured axial velocity traces at the tip of the first rotor inlet during stall inception (Silkowski, 1995)

Table 2 Comparison of key features of the short wavelength stall inception for the GE matched configuration

	Measurement	Computation
Stall Inception Route	Spike	Spike
Rotating Speed of Spike	70-73%	83%
Rotating Speed of Final Stall Cell	45%	20%
Transition Time (rotor revolutions)	about 3	about 3

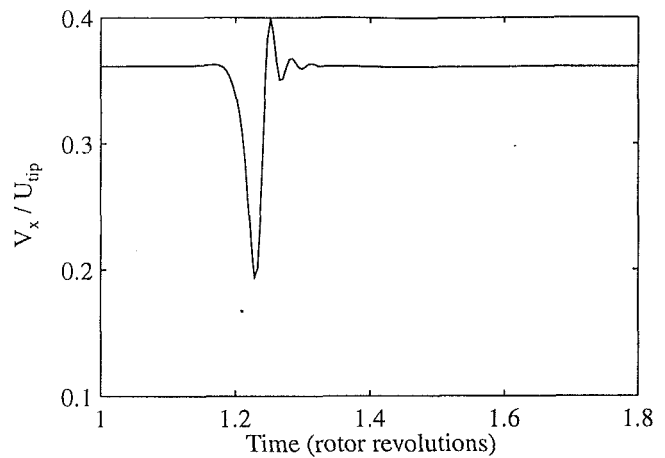Fig. 10 Computed velocity trace showing a localized stall cell

The computed results show the time sequence for short-wavelength stall inception events. The three-dimensional spike grows in amplitude until it triggers the formation of an incipient long-wavelength disturbance, which then grows into the final essentially two-dimensional stall cell. During this process the short-wavelength disturbances travel ahead of the stall cell, due to their faster rotational speed, and eventually decay in the region of higher local mass flow.

Stall in a Mismatched Compressor. Another assessment of the model's ability to describe short-wavelength stall behavior was performed for a mismatched compressor (Silkowski, 1995). By re-staggering the second through fourth rotors of the GE compressor rig so that their stage characteristics peaked at a lower flow coefficient (shown by the solid lines in Fig. 9), one or more fully developed short-wavelength stall cells could be localized in the first stage. Note that stall (defined as when asymmetric flow disturbances were no longer suppressed) occurred at the same flow coefficient as for the matched configuration. The short-length-scale cells were prevented from growing into a long-wavelength stall cell because of the stabilizing influence of the rear stages. The compressor characteristic behaved "progressively" in that the pressure rise increased and decreased smoothly without hysteresis as the overall mass flow was changed, as shown by the solid circles in Fig. 9. The number of localized cells increased from one to twelve as the flow rate decreased, until finally at a sufficiently low flow, a long-wavelength full-scale rotating stall cell developed that extended through the entire compressor.

The computations carried out qualitatively demonstrated the progressive characteristic behavior as shown by the open circles in Fig. 9. Spike disturbances were periodically forced every rotor
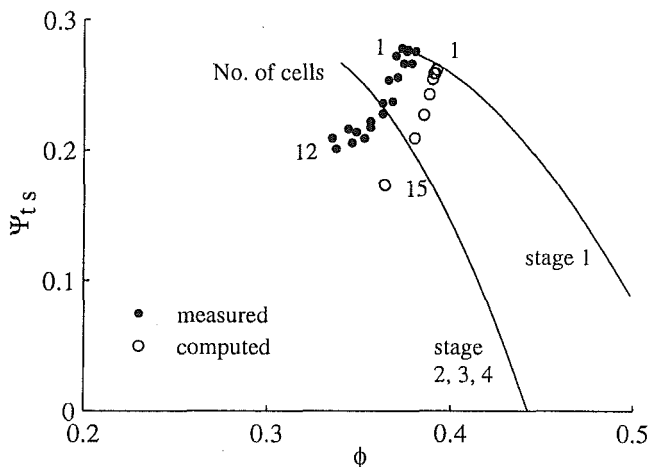
revolution, but only a limited number would grow into fully developed part-span stall cells, each of equal size. As the throttle was closed, the maximum number of disturbances that would develop into stall cells increased, as indicated on the figure. Disturbances imposed in excess of the maximum amount existed only as transients and decayed within one rotor revolution. The computed width of the localized stall cells compared well with the experiment, as indicated by the velocity traces in Figs. 10 and 11. The overall assessment criteria for the mismatched configuration are summarized in Table 3.

The roles of the rotor and stator in short-wavelength stall can be understood better by examining the detailed structure of a localized cell. Figure 12 shows the computed axial velocity contours in a small segment of the first-stage annulus where the cell is localized in the tip region. The flow deficit grows stronger through the rotor and diminishes in the stator, indicating that spikes are supported by the rotor and that the stator has a stabilizing influence.

Switch Between Stall Routes and Unique Incidence for Spikes. Experiments performed by Camp and Day (1998) demonstrated that the route leading to stall could switch from long to short wavelength as the incidence on the first rotor was altered by changes in IGV stagger angle. They also showed that the incidence at the rotor tip is constant for all cases where stall occurred via spikes. Capturing this set of observations with the computational method gives another test of the model's ability to predict short *and* long-wavelength stall events accurately.

Fig. 9 Measured and computed stage characteristics for the GE mismatched compressor. Circles denote the progressive stall, which deviates from the axisymmetric characteristic (solid line).
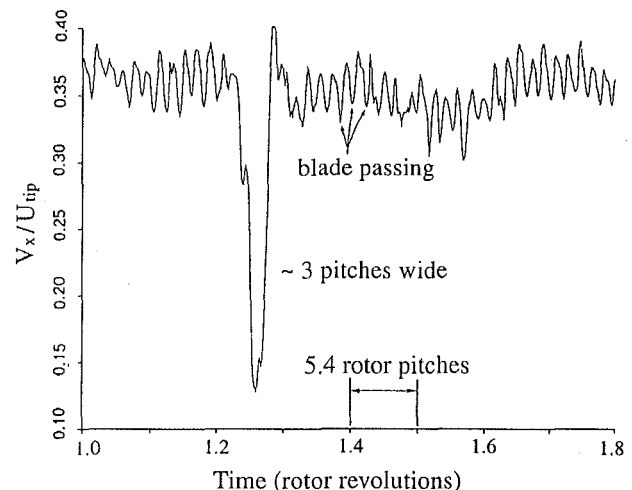

Fig. 11 Measured velocity trace showing a localized stall cell (Silkowski, 1995)

Table 3 Comparison of the short-wavelength progressive stall behavior for the GE mismatched configuration

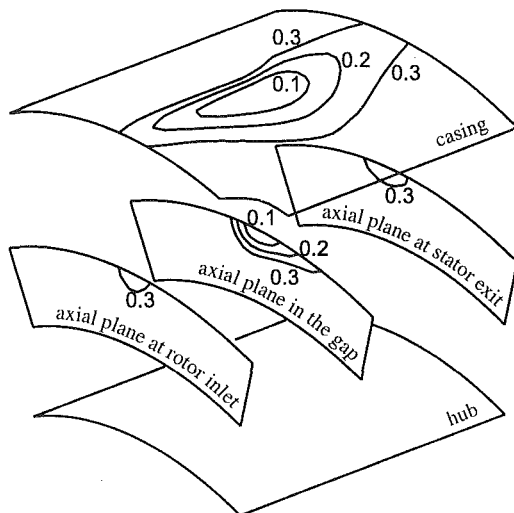|	Measurement	Computation
location	first stage rotor tip	first stage rotor tip
width of spike	2-3 pitches (out of 54)	1/20 annulus (2.7 pitches)
rotating speed	70-73%	83%
progressive stall	yes	yes
no. of stall cells	1 to 12	1 to 15

The simulations were made using the matched GE compressor as the baseline configuration. The amplitude of force impulses was kept constant for all simulations. IGV stagger angle variations were chiefly reflected in the modified first stage pressure rise characteristics. Figure 13 shows these characteristics as well as the stall points, the corresponding incidences at the tip of the first rotor, and the types of stall inception route. The trends are very similar to the observations made by Camp and Day (Fig. 14), in particular the condition of constant rotor incidence value for all cases of short-wavelength stall inception.

In summary, the model reproduced both short-wavelength and long-wavelength stalling trends from previously accepted analytical results and experimental measurements, implying that the body force model gives a good description of both modal and spike-initiated stalling events. The computational method will now be applied to determine the parameters that control multistage compressor instability behavior.
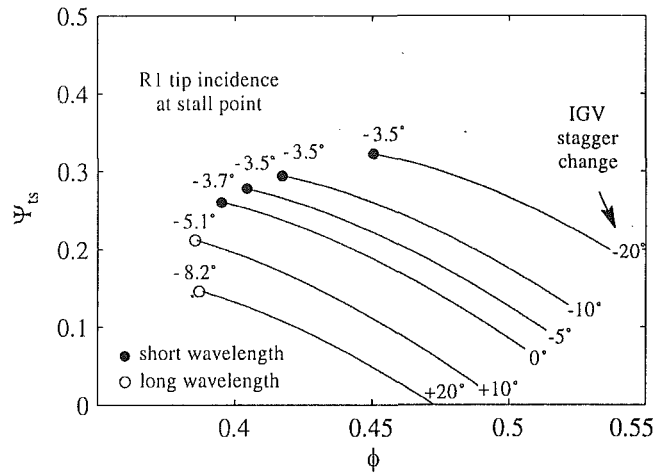
Parametric Study

To identify the conditions that set the stall point of short-wavelength disturbances in a multistage compressor, two aspects of the stall inception were examined: the types of initial flow disturbance, and the geometry of the compressor. The initial disturbances used were both small-amplitude modal perturbations and large amplitude spike-shaped impulses localized to either the tip or hub of the first rotor. The amplitude of the tip-spikes and the rotor in which they appeared were also varied. Finally, the gap lengths between particular blade rows were varied to isolate the effects of different segments of the compressor.

The baseline configuration for all simulations was the GE four-

Fig. 13 First-stage characteristics with the stall point and inception type computed for different IGV staggers

stage compressor described above in the matched configuration. In this section changes to the stall point (δ) are referenced to the computed modal stall point, which was at the peak of the pressure rise characteristic.
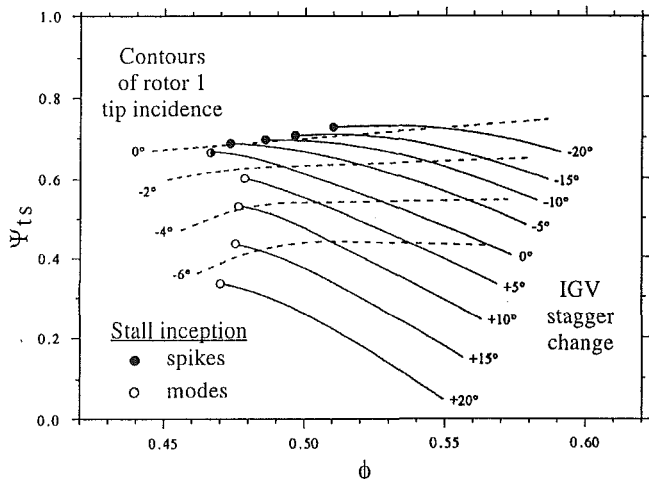
$$\delta = \frac{\phi_{stall} - \phi_{modal\ stall}}{\phi_{modal\ stall}} \qquad (5)$$

A positive δ indicates that stall occurs at an operating point to the right of the peak, i.e., on the negatively sloped part of the overall characteristic.

Type of Initial Disturbances. Stall point and type of stall inception were determined using three types of disturbance to the body force in the first rotor: (1) small amplitude, long wavelength; (2) large amplitude, spike-shaped at the tip; (3) large amplitude, spike-shaped at the hub. The shape and amplitude of these disturbances were the same as those described in the section on "Implementation of the Model."

The results are shown in Fig. 15, which shows the stall inception route and change in stall point for the three disturbance types. Only the tip-spike disturbances led to short wavelength stall inception and the largest loss in stall margin.

Disturbance Amplitude. The effect of the disturbance size on the stalling behavior is shown in Fig. 16. The amplitude has been

Fig. 12 Computed flow coefficient contours of a localized stall cell in the first stage of the GE mismatched configuration. A tangential extent equal to six blade pitches is shown.

Fig. 14 First-stage characteristics with the stall point and inception type indicated for different IGV staggers. Measured by Camp and Day (1998).
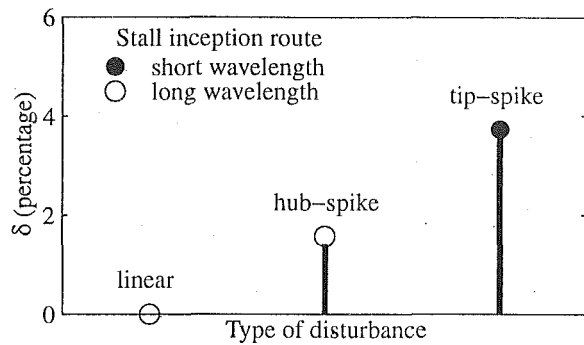
Fig. 15 Changes in stall point and inception type for different types of initial disturbances
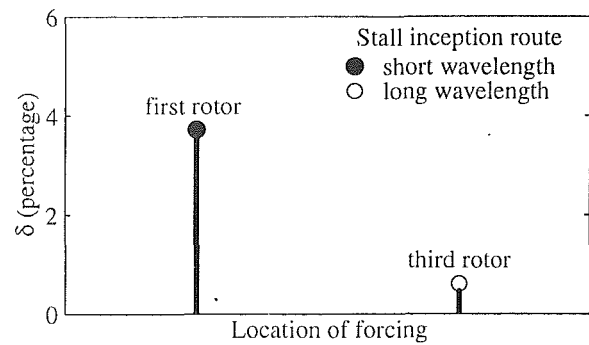

Fig. 17 Changes in stall point and inception type with location of initial spike

normalized by the baseline spike amplitude. The figure shows the following points:

1　Spike disturbances needed to be larger than a threshold amplitude to cause a short-wavelength-type inception. Below this amplitude, modal stall inception occurred.

2　The stall margin decreased as the disturbance amplitude increased. Spike inception always occurred on the negatively sloped part of the pressure rise characteristic.

3　There was an upper limit in the loss of stable flow range due to short wavelength disturbances for this configuration. Above a critical flow coefficient (given by $\delta = 7$ percent) the compressor was stable to all spike disturbance sizes tried.

The computations show that compressor instability involving short-length-scale disturbances is inherently nonlinear, in contrast with long-wavelength stall behavior, which is essentially a linear phenomenon.

Disturbance Location. In the matched compressor experiments, the short-wavelength stall cells were always initiated in the first-stage rotor. It was of interest to use the model to examine what happens when spikes are imposed in a rotor further downstream. The stalling behavior induced by tip-spikes in the third-stage rotor is compared to the baseline in Fig. 17. Only disturbances in the first-stage rotor were found to lead to short-wavelength stall inception.

An explanation for this was offered by Camp and Day (1998) who argued that rotors other than the first tended to be slightly less loaded when off-design because drops in the axial velocity increased the deviation of downstream stators more than that of the inlet guide vane. However, in the computed flow fields, the axial velocity profiles and incidence angles at all rotor inlets were essentially the same, so the loading differences between the first

rotor and subsequent rotors were small. A different explanation for why spikes select the first rotor, at least in the present configuration, is suggested in the next section.

Gap Lengths Between Blade Rows. In the GE compressor, the first rotor was unique in that the IGV-R1 gap was three times the length of all other gaps. The effect of rotor–stator gap length on the type and location of stall inception was numerically examined by independently varying the IGV-R1, R1-S1, and S1-R2 gaps. For all studies, the tip-spike impulses were imposed in the first rotor.

The results are shown in Fig. 18, which indicates that the stall point was set only by the spacing between the first rotor and its adjacent stators. Changing the S1-R2 gap had no effect on stall. Increasing the IGV-R1 or R1-S1 gaps destabilized the compressor to short-length-scale disturbances. Bringing the IGV or first stator sufficiently close to the first rotor suppressed the development of spikes entirely, so that stall occurred via long-wavelength inception. This effect supports the notion that stators have a stabilizing influence on spikes.

Similar studies done for the mismatched GE configuration gave the same qualitative trends. It was also found that the size of the localized short-wavelength stall cells increased with increasing R1-S1 gap, but were unaffected by the S1-R2 gap length.

All computations indicated that short-length-scale stalling behavior in a particular rotor was set by the adjacent blade row components, and not by the design of the rest of the compressor. The preference for spike stall in the first-stage rotor is predominantly due to the relatively large IGV-R1 gap as compared to the gaps within the downstream stages.

Discussion

We have demonstrated that a computational model based on an infinite blade number representation of the blade rows is capable of
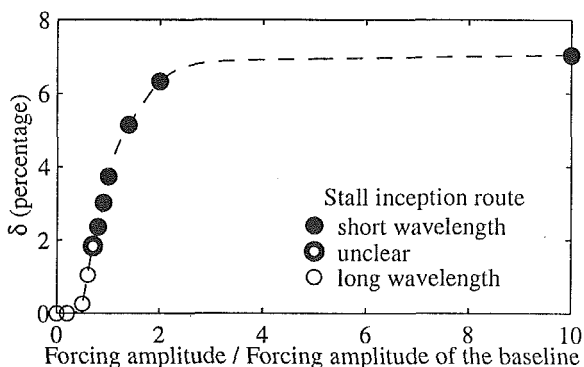

Fig. 16 Effects of initial spike forcing amplitude on stall point and inception type
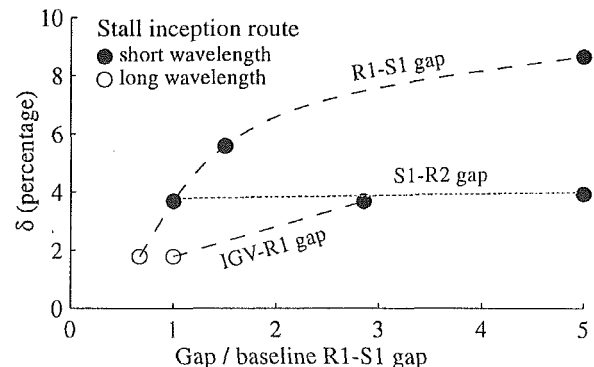

Fig. 18 Effects of IGV-R1, R1-S1, and S1-R2 gap lengths on stall point and inception type

capturing the experimentally observed characteristics of short-wavelength stall events. The significant features of this model are that it is three dimensional, nonlinear, represents each blade row individually, and uses finite amplitude spike-shaped disturbances to perturb the flow. During the model's development, it was found that short-length-scale stall behavior would not be exhibited if any one of these aspects was missing. A model with these elements is therefore the simplest one that can be used to calculate the short-wavelength stalling process. The adequacy of the model, which uses an infinite number of blade assumptions, indicates that the short-length-scale stall inceptions, observed by Camp and Day (1998), Day (1993), Day et al. (1999), Park (1994), and Silkowski (1995), can be viewed as the consequences of compression systems subjected to localized finite amplitude disturbances, and modeled without resolving the detailed flow structures within blade passages.

Up to now we have not inquired as to the physical origin of the finite amplitude tip-spike disturbances observed by Park (1994). Insight is provided by the eight-blade passage isolated rotor calculations performed by Hoying et al. (1999). Simulations at stall demonstrated that the motion of the tip vortex in and out of a rotor passage produced spike-shaped disturbances. It would seem that discrete blade passage events, such as tip vortex dynamics, are likely the sources of the short-length-scale disturbances. These need to be computed with a discrete blade model, but the infinite blade number compressor model is adequate for determining the overall effect of these disturbances on compressor stability.

Although it can be presumed that disturbances exist within the blade passages of each bladerow in a multistage compressor, the amplitude of these disturbances can be of varying magnitude. As shown in this paper, the amplitude of disturbances can affect the instability point. Recognizing where these disturbances with a threshold magnitude for initiating the instability exist, and only applying body force impulses to these stages, is an integral part of using the new model for compressor stall prediction. This aspect differs from linearized analyses, which presume that infinitesimal disturbances of all wavelengths are always present through the compressor. Further research on the physical sources of such disturbances, and the conditions for setting their amplitude, are needed to provide a rigorous basis for choosing proper disturbances.

Results from this paper indicate that the growth or decay of short-length-scale disturbances in a rotor is dependent on the characteristics of that rotor and its neighboring stators. We refer to these three blade rows as a component group. Changing the spacing of the blade rows within a component group did affect stall point, the shape of the stall cell, and stall route; however, changing the distance between the component group with spike forcing and the other blade rows had no effect. Further evidence comes from the GE assessment calculations, which showed the first stage stalled via spikes at the same flow coefficient whether the downstream stages were mismatched or not. To find the stall point of a compressor with spike disturbances, it is thus only necessary to model each individual component group containing the spikes.

The model developed here may be used to determine specific short-wavelength stall criteria, which would be valuable for compressor design. The observation by Camp and Day (1998) that the rotor incidence at stall is constant for different blade loadings is augmented by our result that this incidence angle depends on the gaps within the component group. Further calculations may determine the link between blade spacing and the critical rotor incidence, and thus develop explicit rules for the prediction of short-length-scale stall in general component group designs.

Summary and Conclusions

A three-dimensional computational model was developed for simulating the development of both long and short-wavelength compressor instabilities. Individual blade rows were represented by a body force formulated in terms of the blade's pressure rise and turning characteristics. The ability of the model to capture observed behavior was assessed against experimental measure-

ments and analytical results. The model has been used in a set of simulations to explore the parametric trend of the instability behavior of a four-stage low speed compressor.

The following conclusions were deduced from the simulations:

1 The necessary ingredients of the model are a three-dimensional, nonlinear, row-by-row representation of compressor response to finite amplitude disturbances. The short-length-scale stalling process cannot be described if any one of these is missing.

2 Localized disturbances of sufficient amplitude (large enough to effect zero pressure rise in the tip) are required to initiate the short-wavelength route to rotating stall.

3 The computations show instability occurring on the negatively sloped part of the overall compressor characteristic, in agreement with experimental measurements. This is in direct contrast to the predictions of the modal type of analyses, in which the instability will occur at the peak of the characteristic.

4 The growth or decay of small-length-scale disturbances in a rotor is determined by the design characteristics of the isolated component group consisting of the rotor and its adjoining stators.

5 The point at which stall occurs (i.e., propagating asymmetrical disturbances do not decay) via the short-wavelength route is set by the most unstable component group where large amplitude spike disturbances are present.

6 Closing the rotor–stator gaps within the most unstable component group suppresses the growth of short-wavelength disturbances, thereby improving compressor stability.

References

Billet, G., Huard, J., Chevalier, P., and Laval, P., 1988, "Experimental and Numerical Study of the Response of an Axial Compressor to Distorted Inlet Flow," ASME *Journal of Fluids Engineering,* Vol. 110, pp. 355–360.

Camp, T. R., and Day, I. J., 1998, "A Study of Spike and Modal Stall Phenomena in a Low-Speed Axial Compressor," ASME JOURNAL OF TURBOMACHINERY, Vol. 120, pp. 393–401.

Day, I. J., 1993, "Stall Inception in Axial Flow Compressors," ASME JOURNAL OF TURBOMACHINERY, Vol. 115, pp. 1–9.

Day, I. J., Breuer, T., Escuret, J., Cherrett, M., and Wilson, A., 1999, "Stall Inception and the Prospects for Active Control in Four High-Speed Compressors," ASME JOURNAL OF TURBOMACHINERY, Vol. 121, pp. 18–27.

Escuret, J. F., and Garnier, V., 1994, "Numerical Simulations of Surge and Rotating Stall in Multi-Stage Axial-Flow Compressors," AIAA Paper No. 94-3202.

Gong, Y., 1998, "A Computational Model for Rotating Stall and Inlet Distortions in Multi-stage Compressors," Ph.D. Thesis, Massachusetts Institute of Technology.

Greitzer, E. M., 1976, "Surge and Rotating Stall in Axial Flow Compressors, Parts I and II," ASME *Journal of Engineering for Power,* Vol. 98, pp. 190–217.

Haynes, J. M., Hendricks, G. J., and Epstein, A. H., 1994, "Active Stabilization of Rotating Stall in a Three-Stage Axial Compressor," ASME JOURNAL OF TURBOMACHINERY, Vol. 116, pp. 226–239.

Hoying, D. A., Tan, C. S., Vo, H. D., and Greitzer, E. M., 1999, "Role of Blade Passage Flow Structures in Axial Compressor Rotating Stall Inception," ASME JOURNAL OF TURBOMACHINERY, Vol. 121, this issue, pp. 735–742.

Jameson, A., Schmidt, W., and Turkel, E., 1981, "Numerical Solutions of the Euler Equations by Finite Volume Methods With Runge–Kutta Time Stepping Schemes," AIAA Paper No. 81-1259.

Longley, J. P., Shin, H. W., Plumley, R. E., Silkowski, P. D., Day, I. J., Greitzer, E. M., Tan, C. S., and Wisler, D. C., 1996, "Effects of Rotating Inlet Distortion on MultiStage Compressor Stability," ASME JOURNAL OF TURBOMACHINERY, Vol. 118, pp. 181–188.

Longley, J. P., 1997, "Calculating the Flowfield Behaviour of High-Speed Multi-Stage Compressors," ASME Paper No. 97-GT-468.

Marble, F. E., 1964, "Three-Dimensional Flow in Turbomachines," *Aerodynamics of Turbines and Compressors, Vol. X of High Speed Aerodynamics and Jet Propulsion,* Hawthorne, W. R., ed., Princeton University Press, Princeton, NJ, pp. 83–166.

McDougall, N. M., 1988, "Stall Inception in Axial Compressors," Ph.D. Thesis, Cambridge University.

Moore, F. K., 1984, "A Theory of Rotating Stall of Multistage Axial Compressors: Parts I–III," ASME *Journal of Engineering for Gas Turbines and Power,* Vol. 106, pp. 313–336.

Moore, F. K., and Greitzer, E. M., 1986, "A Theory of Post-Stall Transients in Axial Compression Systems: Part I, II," ASME *Journal of Engineering for Gas Turbines and Power,* Vol. 108, pp. 68–76, pp. 231–239.

Park, H. G., 1994, "Unsteady Disturbance Structures in Axial Flow Compressor Stall Inception," Master's Thesis, Massachusetts Institute of Technology.

Silkowski, P. D., 1995, "Measurements of Rotor Stalling in a Matched and a Mismatched Multistage Compressor," GTL Report No. 221, Gas Turbine Laboratory, Massachusetts Institute of Technology.

Tryfonidis, M., Etchevers, O., Paduano, J. D., Hendricks, G. F., and Epstein, A. H., 1995, "Prestall Behavior of Several High-Speed Compressors," ASME JOURNAL OF TURBOMACHINERY, Vol. 117, pp. 62–80.

Vo, H. D., 1999, private communication.

Weigl, H. J., Paduano, J. D., Frechette, L. G., Epstein, A. H., and Greitzer, E. M., 1998, "Active Stabilization of Rotating Stall and Surge in a Transonic Single Stage Axial Compressor," ASME JOURNAL OF TURBOMACHINERY, Vol. 120, pp. 625–636.

Wisler, D. C., 1981, "Core Compressor Exit Stage Study, Volume IV—Data and Performance Report for the Best Stage Configuration," NASA CR-165357, NASA Lewis Research Center.

APPENDIX

Formulation of the Body Force Field

The derivation of the body force field used to represent the blade regions in the model is presented here. The forces, calculated separately for each blade row, must satisfy the following general requirements:

1 For steady-state axisymmetric flow, the blade row model must reproduce the correct overall pressure rise and turning angle.

2 The body forces must be able to locally respond to unsteady three-dimensional flow variations.

The body force distribution depends on the following three characteristics of the blade row: the total pressure rise, $\Psi_n(\phi, r)$, the exit flow angle, $\beta_{exit}(\phi, r)$, and the local angle along the blade camber line, $\alpha(x, r)$.

For this particular GE compressor, it is convenient to break the body force vector into two parts, one turning the flow without work being done, the other solely producing the total pressure rise:

$$\mathbf{F} = \mathbf{F}_{turning} + \mathbf{F}_{\Psi_{tt}} \tag{6}$$

The radial component of the body force, F_r, is assumed to be zero since the blades have little radial skewness. Only the axial component of $\mathbf{F}_{\Psi_{tt}}$ contributes to the pressure rise, so

$$F_{\Psi_{tt},\theta} = 0 \tag{7}$$

$$F_{\Psi_{tt},x}(x, r, \theta) = f(x)\Psi_{tt}(\phi(x, r, \theta), r) \tag{8}$$

where

$$\int_{leading\ edge}^{trailing\ edge} f(x)dl = 1. \tag{9}$$

$f(x)$ is a function used to distribute the force along the streamlines (dl) through the blade region. The distribution function is forced to be small near the leading and trailing edges to reduce numerical oscillations. Equation (9) is simplified by assuming the streamlines are parallel to the axis (i.e., $dl = dx$) since all compressors used in this paper have a high hub-to-tip ratio.

$\mathbf{F}_{turning}$ is constructed so the flow turns toward the camber line angle in the relative frame of the blade row. The tangential component of the force is given by

$$F_{\theta,turning} = CV_x(r\Omega + V_x \tan(\alpha) - V_\theta). \tag{10}$$

The constant C is calibrated to produce the correct deviation angle at the design flow coefficient. $\mathbf{F}_{turning}$ is chosen normal to the local velocity $\mathbf{V}$ so that it does not affect the total pressure. Therefore,

$$F_{turning,x} = \frac{V_x}{V_\theta} F_{turning,\theta}. \tag{11}$$